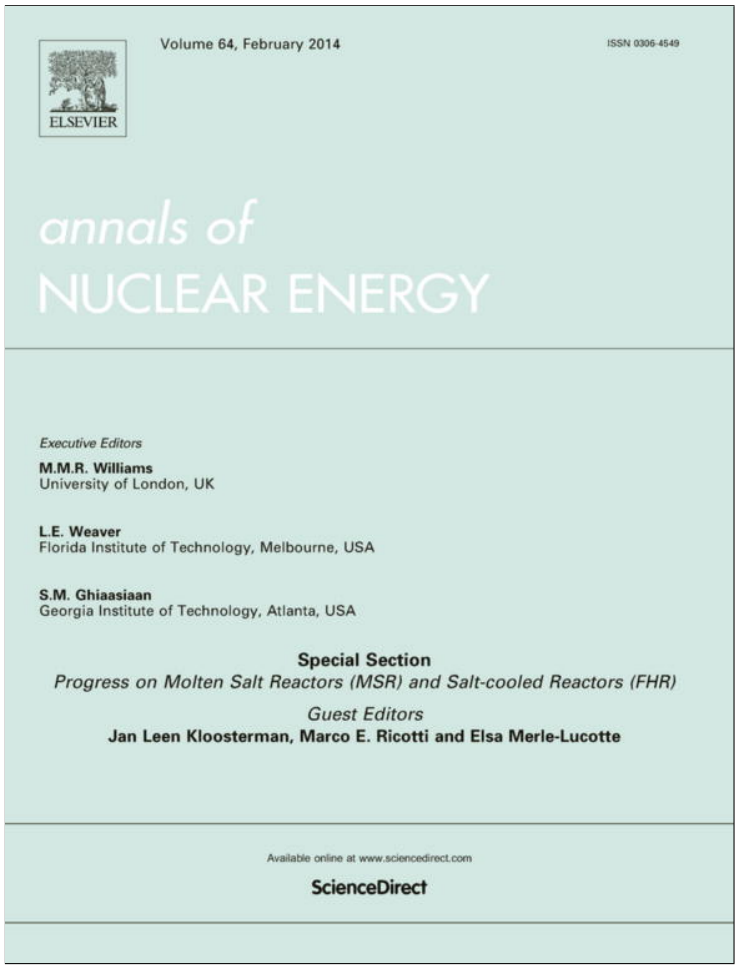

Annals of Nuclear Energy 64 (2014) 191–200

Contents lists available at ScienceDirect

Annals of Nuclear Energy

journal homepage: www.elsevier.com/locate/anucene

Non-linear simulation and control of xenon induced oscillations in Advanced Heavy Water Reactor

R.K. Munje [a], B.M. Patre [a], A.P. Tiwari [b,*]

[a] Department of Instrumentation Engineering, Shri Guru Gobind Singhji Institute of Engineering and Technology, Vishnupuri, Nanded 431 606, India
[b] Reactor Control Division, Bhabha Atomic Research Centre, Trombay, Mumbai 400 085, India

ARTICLE INFO

Article history:
Received 21 April 2013
Received in revised form 17 September 2013
Accepted 25 September 2013
Available online 26 October 2013

Keywords:
Advanced heavy water reactor
Spatial stabilization
Spatial oscillations
Vectorization
Thermal hydraulics
Mathematical model

ABSTRACT

The physical dimensions and the reactivity feedbacks of Advanced Heavy Water Reactor (AHWR) are such that, it is susceptible to xenon induced spatial oscillations. If these oscillations are not controlled, the power density and the rate of change of power at some locations in the reactor core may exceed their respective thermal limits, resulting into increased chances of fuel failure. Hence, it is essential to suppress xenon oscillations and achieve spatial stabilization of AHWR. Reactor core of AHWR is divided into 17 non-overlapping nodes. Non-linear model of AHWR is characterized by 90 first order differential equations. Total reactor power and 17 nodal powers are output variables. Four voltage signals to the Regulating Rods (RRs) and a feed flow rate are input variables. Applying a highly developed simulation is necessary for analysis and control of spatial oscillations developed in AHWR for safe operation. In this paper, after carrying out stability analysis, a control strategy based on feedback of total power and nodal powers in which RRs are placed is presented for spatial control of AHWR. For the same, a vectorized non-linear model of AHWR is developed and is implemented in the MatLab/Simulink environment which helps to understand the relationship between different variables of the system in a better way. With the proposed controller, non-linear model of AHWR is simulated and results are generated for different transient conditions. The behavior of delayed neutron precursor and xenon concentrations is also analyzed for each transient. From the simulation results, performance of the proposed controller is found to be satisfactory.

1. Introduction

Design of the robust controller for spatial power control of nuclear reactor depends very heavily on how well we know the dynamics of the nuclear reactor. Dynamics refer to interactions among different system variables. To investigate the dynamics and to explore modern control system techniques for nuclear reactor control system design, it is important to have a reactor model that not only captures the essential features but also is moderate in its complexity for applying control system design and simulation technique (Javidnia et al., 2009). Nuclear reactors of small and medium size are generally described by the point-kinetic model which characterizes every point in the reactor by an amplitude factor and a time independent spatial shape function. This model is, however, not valid in case of large reactors, like Pressurized Heavy Water Reactor (PHWR) and Advanced Heavy Water Reactor (AHWR), because the flux shape undergoes appreciable variation with time and space (Shimjith et al., 2011). For explicit consideration of the variation of the flux shape it is necessary to have suitable model of nuclear reactor. Further, because of the potential for accidents or sabotage at nuclear power plants, the operation and control of these plants represents a complex problem. Several safety and control features are engineered at the design stage and operational policies are incorporated to avoid accidental release of radioactivity to the general population. The problems are further complicated in case of large nuclear reactor (Tiwari, 1999). Because of safety critical nature of the nuclear reactor, wide variety of computer codes have been developed and implemented in the form of off-line computer programs to study the behavior of plant in various postulated accident conditions (Javidnia et al., 2009; Seyed, 2012; Tiwari, 1999). In this paper, vectorized non-linear model of AHWR is developed and implemented by Simulink tool kit of MatLab software to explore dynamic behavior for control system studies. Also, the existence of spatial oscillations in AHWR is studied for control purposes, since, such oscillations are highly detrimental for safe operation of large nuclear reactor. In (Shimjith et al., 2011) it is shown that, the feedback of total power and all the nodal power distribution signals are required to suppress xenon induced oscillations. However, in this paper it is demonstrated that, to suppress xenon oscillations, feedback of total power and

* Corresponding author. Tel.: +91 22 25595178; fax: +91 22 25505151.
E-mail addresses: ravimunje@yahoo.co.in (R.K. Munje), bmpatre@ieee.org (B.M. Patre), aptiwari@barc.gov.in (A.P. Tiwari).

0306-4549/$ - see front matter © 2013 Elsevier Ltd. All rights reserved.
http://dx.doi.org/10.1016/j.anucene.2013.09.038

Nomenclature

Notations

C	precursor concentration
x	exit mass quality
E_{eff}	thermal energy liberated/fission, J
α	coupling coefficient
E_n	identity matrix of dimension n
β	delayed neutron fraction
H	position of regulating rod, % in
γ	fraction fission yield
I	iodine concentration
λ	decay constant
P	steam drum pressure, Mpa
ℓ	the prompt neutron life-time, s
V	volume, m^3
ρ	reactivity, k
W	fission power, MW
σ_a	microscopic absorption cross-section, cm^2
X	xenon concentration
Σ_a	macroscopic absorption cross-section, cm^{-1}
h	enthalpy, kJ/kg
Σ_f	macroscopic fission cross-section, cm^{-1}
q	mass flow rate, kg/s
κ	constant of regulating rod position
v	voltage signal to RR drive, V
δ	deviation parameter

Subscripts

C	precursor
d	downcomer
H	position of regulating rod
f	feed water, fission
I	iodine
i, j	node number
P	power
k	regulating rod number
R	regulating rod
r	riser
T	total power
s	steam
X	xenon
w	water
c	vaporization
x	exit quality

only nodal power distribution signals where RRs are placed would be sufficient. The effectiveness of proposed control strategy is established through non-linear simulation results.

The rest of the paper is organized as follows. In Section 2 brief overview of AHWR is given. Mathematical model of AHWR is discussed in Section 3. In Section 4 vectorized model of AHWR is developed and is implemented in Simulink environment. Section 5 presents proposed control strategy. Non-linear simulation results are discussed in Section 6 and finally paper is concluded in Section 7.

2. Brief overview of AHWR

In India, Advanced Heavy Water Reactor, a 920 MW (thermal), vertical pressure tube type reactor, moderated by heavy water, cooled by boiling light water under natural circulation is designed using thorium-based technology as a third step of Indian nuclear power program. The AHWR is fueled with (Th–^{233}U) O_2 and (Th–Pu) O_2 pins (Sinha and Kakodkar, 2006). The 3.5 m long active core of AHWR has 513 lattice locations. Out of these, fuel assemblies occupy 452 locations and remaining 24 locations are reserved for reactivity control devices consisting of 8 Absorber Rods (ARs), normally fully inside the core, 8 Shim Rods (SRs), normally fully out of the core, and 8 Regulating Rods (RRs). RRs are used for fine adjustments in reactor power and they remain partially inside the reactor core under normal operating conditions. Out of the eight RRs, four are available for automatic control whereas, the remaining four are under manual operation. The remaining lattice locations are occupied by the shutdown system-1 consisting of 37 Shut-Off Rods (SORs). The neutron flux is measured using out-of-core ion chambers as well as in-core detectors. The total power of the reactor is inferred from ion chambers in low power range and from in-core detectors in power range. In-core detectors, however, are provided primarily for monitoring of spatial flux distribution in the core (Shimjith et al., 2008; Shimjith et al., 2010; Sinha and Kakodkar, 2006). The Main Heat Transport (MHT) system of AHWR consists of 452 coolant channels in reactor core, equal number of tail pipes, 4 horizontal cylindrical steam drums, 16 downcomers, an inlet header and 452 inlet feeders as shown in Fig. 1. Coolant starts boiling in the reactor core by absorbing the fission heat. Coolant channels belonging to each quadrant of the reactor core are connected to separate steam drums through individual tail pipes. The coolant circulation is driven by natural convection through tail pipes to steam drum at 7 MPa. Steam–water phase separation and feed water mixing takes place inside the steam drums. The steam is fed to the turbine whereas, the sub-cooled water flows back to the coolant channels through the 4 downcomer pipes to a common inlet header. Individual coolant channels of the core are fed from this common header through individual feeder pipes (Sinha and Kakodkar, 2006; Shimjith et al., 2008; Gaikwad et al., 2009; Shimjith et al., 2011). AHWR has a significant degree of coupling between the neutronics and the two-phase thermal hydraulics. The physical dimensions of AHWR are large compared to the neutron migration length in the core, making it susceptible to xenon induced spatial oscillations (Duderstadt and Hamilton, 1975). Further, situations such as on-line refueling might cause transient variations in flux-shape from the nominal flux-shape. Analysis of such situations can be done by developing a suitable vectorized model of AHWR in Simulink environment.

3. Mathematical model of AHWR

Mathematical model of AHWR is developed in Shimjith et al. (2008); Shimjith et al. (2010) using separate models for core neutronics and for thermal hydraulics of MHT system.

3.1. Core neutronics model

The simplified core neutronics model is obtained by nodal approach, based on finite difference approximation of the two group diffusion equations and the associated equation for an effective single group of delayed neutron precursor's concentration. Seventeen fictitiously divided nodes, as given in Fig. 2, are considered as seventeen small cores, each of which is coupled to its

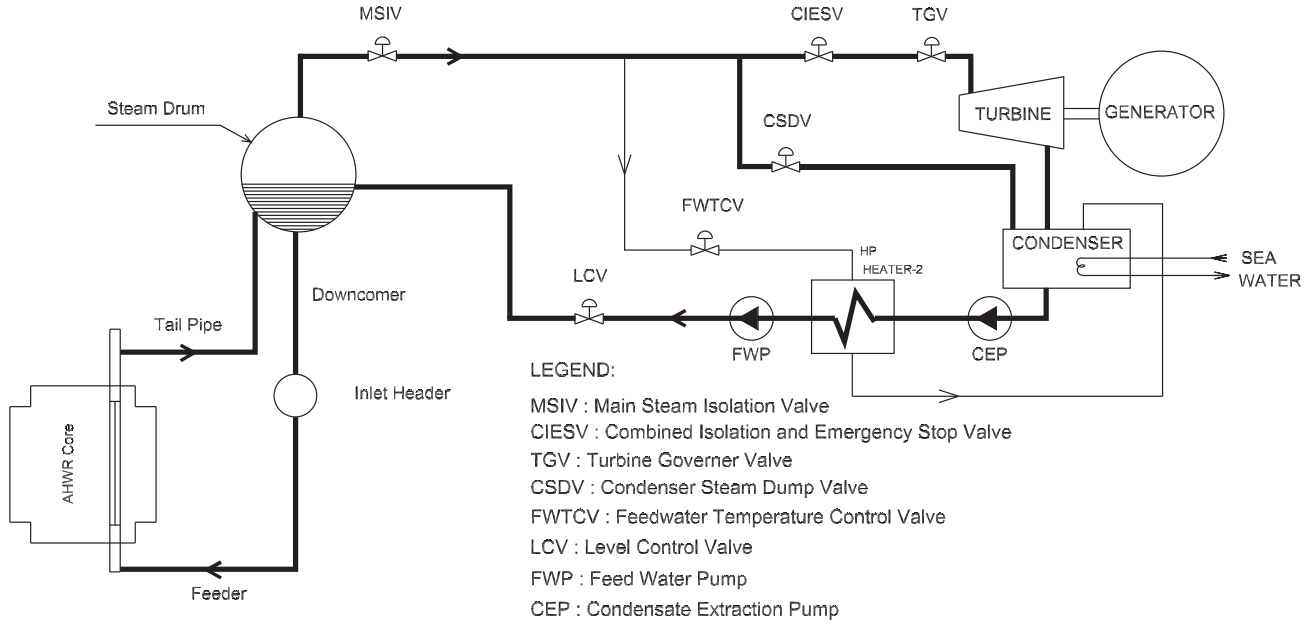

Fig. 1. Main heat transport system of AHWR (Shimjith et al., 2011).

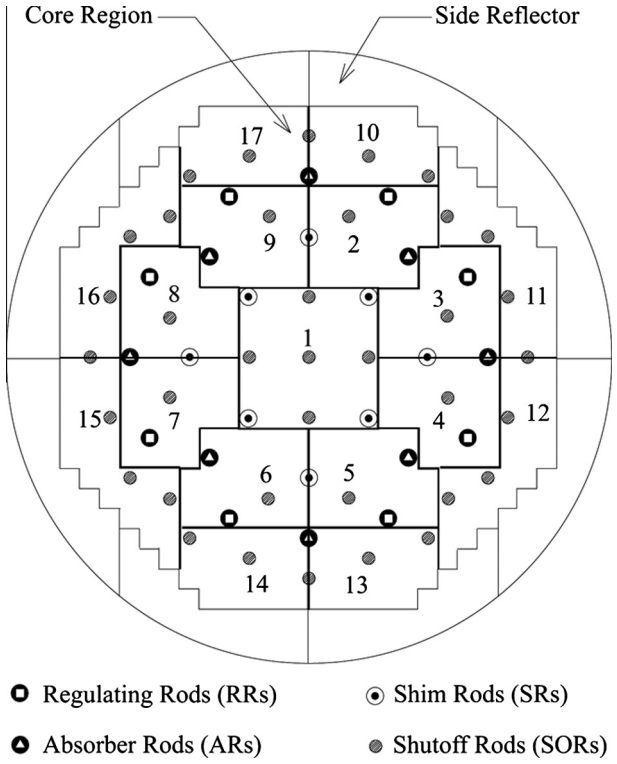

Fig. 2. 17 nodes AHWR scheme.

neighboring nodes through neutron diffusion. The following non-linear equations constitute the neutronics model of the reactor core without internal reactivity feedback.

$$\frac{dW_i}{dt} = (\rho_i - \alpha_{ii} - \beta)\frac{W_i}{\ell} + \sum_{j=1}^{17}\alpha_{ji}\frac{W_j}{\ell} + \lambda C_i, \tag{1}$$

$$\frac{dC_i}{dt} = \frac{\beta}{\ell}W_i - \lambda C_i \quad i = 1,2,\ldots,17 \tag{2}$$

where α_{ji} and α_{ii} denote the coupling coefficients between jth and ith nodes and self coupling coefficients of ith node respectively, β and λ are respectively effective one group delayed neutron yield and decay constant, ℓ is the neutron lifetime and W_i and C_i are the nodal power level and the effective one group delayed neutron precursor concentration of ith node respectively.

The most important fission product poison is xenon because of its exceptionally large capture crosssection for thermal neutrons with half life of 9.2 h. Main proportion of this isotope in a reactor originates from radioactive decay of iodine with half life of 6.7 h (Duderstadt and Hamilton, 1975). To formulate xenon reactivity feedback, iodine and xenon dynamics in each node are represented as

$$\frac{dI_i}{dt} = \gamma_I \Sigma_{f_i} W_i - \lambda_I I_i, \tag{3}$$

$$\frac{dX_i}{dt} = \gamma_X \Sigma_{f_i} W_i + \lambda_I I_i - (\lambda_X + \bar{\sigma}_{X_i} W_i) X_i \tag{4}$$

where γ_I and γ_X are fission yields of iodine and xenon respectively, λ_I and λ_X are respectively decay constants of iodine and xenon and $\bar{\sigma}_{X_i} = \sigma_{X_i}/E_{eff}\Sigma_{f_i}V_i$; I_i denotes iodine concentration and X_i the xenon concentration of ith node. Also, E_{eff} is energy liberated in each fission, V_i is the node volume and Σ_{f_i} is thermal neutron fission cross-section of ith node.

RRs are driven by the respective reversible variable speed type three phase induction motor and static frequency converter. The speed of RR is directly proportional to the voltage applied to the drive motor, and it is given by

$$\frac{dH_k}{dt} = \kappa v_k \quad k = 2,4,6,8; \tag{5}$$

where v_k is control signal applied to the RR drive in the range of ±1 V, κ is a constant having value 0.56 and H_k is '% in' position of RR of kth node. Differential Eqs. (1)–(5) characterize the nodal model of AHWR core neutronics. The neutronic parameters, nodal volumes, cross-sections and nodal powers under full power operation and coupling coefficients are given in (Shimjith et al., 2011) and the same are used for the simulation.

3.2. Thermal hydraulics model

Thermal hydraulics model of MHT system of AHWR has been developed by evolving separate models for reactor core thermal hydraulics and for the steam drums, and afterwards clubbing them together (Astrom and Bell, 2000; Shimjith et al., 2008) as given below.

3.2.1. Core thermal hydraulics

A thermal hydraulics model of the reactor core is obtained assuming an equivalent coolant channel for each node, ignoring the pressure drops in downcomers, feeders and tail pipes, and taking uniform distribution of nodal power along the flow axis. Also, the steam quality is considered to be uniformly increasing along the axial length in the channels after the point of onset of boiling. Now, applying mass and energy balance to the boiling section and solving them together, the core thermal hydraulics model is written as

$$e_{vp_i}\frac{dP}{dt}+e_{vx_i}\frac{dx_i}{dt}=W_i-q_{d_i}(h_w-h_d)-x_ih_cq_{d_i} \tag{6}$$

where P is drum pressure, h_w, h_d and h_c are water, downcomer and condensation enthalpies respectively, x is the average exit quality, q_{d_i} is flow rate of the coolant entering the ith node through downcomer and e_{vp_i} and e_{vx_i} are constants of ith node.

3.2.2. Steam drums

A simple lumped model of the steam drums is developed assuming that carry over and carry under effects are insignificant; a mixture of saturated water and steam enters the steam drum and subcooled water leaves steam drum into the reactor core; and average values of density and enthalpy of the water in the steam drum have been considered. Mass and energy balance equations of the steam drums are respectively represented by

$$e_{pv}\frac{dV_w}{dt}+e_{pp}\frac{dP}{dt}=-\sum_{i=1}^{17}(q_{d_i}-q_{r_i})+q_f-q_s \tag{7}$$

$$e_{xv}\frac{dV_w}{dt}+e_{xp}\frac{dP}{dt}=q_fh_f+xq_rh_s+(1-x)q_rh_w-q_dh_d-q_sh_s \tag{8}$$

where q_f, q_s, q_r and q_d are average values of feed water, steam, saturated steam and subcooled water flow rates respectively and V_w is the volume of water in the steam drum. Finally applying energy balance equation to water volume in steam drum yields

$$e_{p_i}\frac{dP}{dt}+e_{v_i}\frac{dV_w}{dt}+e_{x_i}\frac{dh_d}{dt}=q_fh_f+(1-x)q_rh_w-q_dh_d. \tag{9}$$

Complete thermal hydraulics model is given by set of Eqs. (6)–(9). Further, drum water volume and pressure are being regulated at respective set points by plant control system. Hence, derivatives of P and V_w vanish from Eqs. (6)–(9). The above equations therefore reduce to

$$e_{vx_i}\frac{dx_i}{dt}=W_i-q_{d_i}(h_w-h_d)-q_{d_i}x_ih_c, \tag{10}$$

$$e_{x_i}\frac{dh_d}{dt}=q_f(\hat{k}_2h_f-\hat{k}_1)-q_d(\hat{k}_2h_d-\hat{k}_1) \tag{11}$$

where $\hat{k}_2=\frac{h_s}{h_c}$ and $\hat{k}_1=h_w\hat{k}_2$. In (Shimjith et al., 2011), values of e_{vx_i} and e_{xi} are given and the same are used here. The coolant flow rate through the channels is the function of normalized nodal powers, given as

$$q_{d_i}=\left\{k_1\left[\frac{W_i}{W_{i_0}}\right]^3+k_2\left[\frac{W_i}{W_{i_0}}\right]^2+k_3\left[\frac{W_i}{W_{i_0}}\right]+k_4\right\}q_{d_{i_0}} \tag{12}$$

where $k_1=0.2156$, $k_2=-0.5989$, $k_3=0.48538$ and $k_4=0.8988$. W_{i_0} denotes the power produced by ith node under full power operation and $q_{d_{i_0}}$ is the corresponding coolant flow rate.

3.3. Reactivity feedbacks

The reactivity term ρ_i in (1) is expressed as $\rho_i=\rho_{i_u}+\rho_{i_X}+\rho_{i_\alpha}$, where ρ_{i_u} is the reactivity introduced by the control rods, ρ_{i_X} is the reactivity feedback due to xenon and ρ_{i_α} is the reactivity feedback due to coolant void fraction. The reactivity contributed by the movement of the RRs is expressed as

$$\rho_{i_u}=\begin{cases}(-10.234H_i+676.203)\times10^{-6}, & \text{if } i=2,4,6,8\\ 0 & \text{elsewhere.}\end{cases} \tag{13}$$

The xenon reactivity feedback in node i can be expressed as

$$\rho_{i_X}=\frac{\bar{\sigma}_{X_i}X_i}{\Sigma_{a_i}}. \tag{14}$$

The reactivity contribution by the coolant void fraction is

$$\rho_{i_\alpha}=-5\times10^{-3}(9.2832x_i^5-27.7192x_i^4+31.7643x_i^3-17.7389x_i^2+5.2308x_i+0.0792). \tag{15}$$

Eqs. (1)-(5), (10) and (11) constitute complete coupled neutronics thermal hydraulics model of AHWR. Seventeen equations each of power, delayed neutron precursor, xenon, iodine concentrations and exit quality, four equations of RR positions and one equation of downcomer enthalpy results into 90 non-linear first order differential equations. Four control signals to RRs and a feed flow rate are input variables with seventeen nodal powers and a total (global) power as output variables. The nodal powers and coolant flow rates are constants as given in (Shimjith et al., 2011) under steady state operation. The equilibrium positions of all RRs is 66.1% inside the core. Coolant enters the core at a temperature of 260 °C and feed water enters the steam drum at 130 °C. The operating pressure of the main heat transport system is 7 MPa. Equilibrium values of other variables like delayed neutron precursor, iodine and xenon concentrations, exit quality and feed flow rate can easily be computed from the steady state forms of respective equations.

3.4. Linearization and state-space representation

The set of non-linear equations given by (1)-(5), (10) and (11) can be linearized around steady state operating conditions $(H_{k_0}, X_{i_0}, I_{i_0}, h_{d_0}, C_{i_0}, x_{i_0}, W_{i_0})$ and the linear equations so obtained can be represented in standard state-space form. For this, define the state vector as

$$\mathbf{z}=\left[\mathbf{z}_H^T\ \mathbf{z}_X^T\ \mathbf{z}_I^T\ \delta h_d\ \mathbf{z}_C^T\ \mathbf{z}_x^T\ \mathbf{z}_W^T\right]^T \tag{16}$$

where $\mathbf{z}_H=[\delta H_2\ \delta H_4\ \delta H_6\ \delta H_8]^T$ and the rest $\mathbf{z}_\xi=[(\delta\xi_1/\xi_{1_0})\cdots(\delta\xi_{17}/\xi_{17_0})]^T$, $\xi=X,I,C,x,W$, in which δ denotes the deviation from respective steady state value of the variable. Likewise define the input vector as $\mathbf{u}=[\delta v_2\ \delta v_4\ \delta v_6\ \delta v_8]^T$ and output vector as $\mathbf{y}=[y_T\ y_1\ \ldots\ y_{17}]^T$ where $y_T=\sum_{i=1}^{17}\frac{\delta W_i}{\sum_{j=1}^{17}W_{j_0}}$ and $y_i=\frac{\delta W_i}{W_{i_0}}$ correspond to normalized total reactor power and nodal powers respectively. Then the system given by (1)-(5), (10) and (11) can be expressed in standard linear state-space form as

$$\dot{\mathbf{z}}=\mathbf{Az}+\mathbf{Bu}+\mathbf{B}_f\delta q_f \tag{17}$$

$$\mathbf{y}=\mathbf{Mz} \tag{18}$$

where q_f is feed water flow rate. Matrices $\mathbf{A}$, $\mathbf{B}$, $\mathbf{B}_f$ and $\mathbf{M}$ are given in (Shimjith et al., 2011). Six eigenvalues of $\mathbf{A}$ have their real parts positive while four eigenvalues are at the origin, which indicates

instability. Hence, it is necessary to design an effective controller to maintain the total power of the reactor while the xenon induced oscillations are being controlled.

4. Vectorization and implementation of AHWR model in Simulink

The dynamic Eqs. (1)-(5), (10) and (11) can be written in vector/matrix form to implement in MatLab/Simulink environment (MatLab/Simulink Control Design Toolbax user manual, 2009). For that, rearrange Eq. (1) of nodal powers as

$$\frac{dW_i}{dt} = \frac{1}{\ell}\left[\rho_i W_i - \alpha_{ii} W_i - \beta W_i + \sum_{j=1}^{17} \alpha_{ji} W_j + \lambda \ell C_i\right]. \tag{19}$$

In the above equation ℓ, β are constants, ρ_i, α_{ii}, C_i and W_i are column vectors and α_{ji} is a matrix. However, the terms $\rho_i W_i$, $\alpha_{ii} W_i$, βW_i, $\sum_{j=1}^{17} \alpha_{ji} W_j$ and $\lambda \ell C_i$ are all column vectors of same dimensions. If scalar multiplication is denoted by '$\cdot$', element-wise multiplication is denoted by '$\odot$' and array multiplication is denoted by '$*$' then (19) can be rewritten as

$$\frac{dW_i}{dt} = \frac{1}{\ell} \cdot \left[\rho_i \odot W_i - \alpha_{ii} \odot W_i - \beta \cdot W_i + \sum_{j=1}^{17} \alpha_{ji} W_j + (\lambda \ell) \cdot C_i\right]. \tag{20}$$

Above equation is implemented using only one integrator, instead of seventeen different integrators. Simulink of MatLab automatically expands the equation to appropriate size as shown in Fig. 3. Initial value of nodal powers can be inserted in the integrator in vector form by double clicking 'integrator' block.

Similarly, the delayed neutron precursor, iodine, xenon concentrations and rod position dynamics can be structured in vector/matrix form as

$$\frac{dC_i}{dt} = \frac{\beta}{\ell} \cdot W_i - \lambda \cdot C_i, \tag{21}$$

$$\frac{dI_i}{dt} = (\gamma_I \cdot \Sigma_{fi}) \odot W_i - \lambda_I \cdot I_i, \tag{22}$$

$$\frac{dX_i}{dt} = (\gamma_X \cdot \Sigma_{fi}) \odot W_i + \lambda_I \cdot I_i - \lambda_X \cdot X_i - \bar{\sigma}_{Xi} \odot W_i \odot X_i, \tag{23}$$

$$\frac{dH_k}{dt} = \kappa \cdot v_k \quad k = 2,4,6,8; \quad i = 1,2,\ldots,17. \tag{24}$$

After defining vector gains, above Eqs. (21)–(24), can be easily realized in Simulink as a core neutronics subsystem block, as depicted in Fig. 4. In the similar manner, the thermal hydraulics model involving dynamics of exit quality and downcomer enthalpy, given by (10) and (11) are represented in vectorized form as

$$\frac{dx_i}{dt} = \frac{1}{e_{vx_i}} \odot [W_i - q_{d_i} \cdot (h_w - h_d) - (q_{d_i} \odot x_i) \cdot h_c], \tag{25}$$

$$\frac{dh_d}{dt} = \frac{1}{e_{x_i}} \odot [q_f \cdot (\hat{k}_2 h_f - \hat{k}_1) - q_d \cdot (\hat{k}_2 h_d - \hat{k}_1)] \tag{26}$$

and employed in Simulink. The instantaneous coolant flow rate through the channels can be evaluated as per (12). Reactivity on account of RR movements is the function of its position as defined by (5) and (13). These two equations can be collectively implemented. All these equations can be combined together, in the form of different subsystems, considering proper relationship between different variables and reactivity feedbacks, to form complete AHWR model. This model eventually leads to an automatic program that solves non-linear Eqs. (1)-(5), (10) and (11) including reactivity feedbacks given by (13)–(15). Advantages of this type of vectorized non-linear model constructed in Simulink are,

1. it can be used for different types of reactors with different number of nodes, provided that the coupling coefficients matrix and reactivity feedbacks are modeled properly,
2. variations of any variable with respect to time or any other variable can be studied by applying 'scope' block across that variable,
3. visualization of calculation results and their recording for further applications is possible,
4. different methods of solving non-linear differential equations with different step time can be studied and
5. the computations are performed in much less time compared to the transient duration.

5. Proposed control strategy

The linear model of the AHWR given by (17) and (18) presented in Section 3.4, is found to be controllable and observable. Generally feedback of total power is sufficient to control small and medium size nuclear reactors, however, large reactors, like AHWR, require feedback of spatial power distribution alongwith the total power

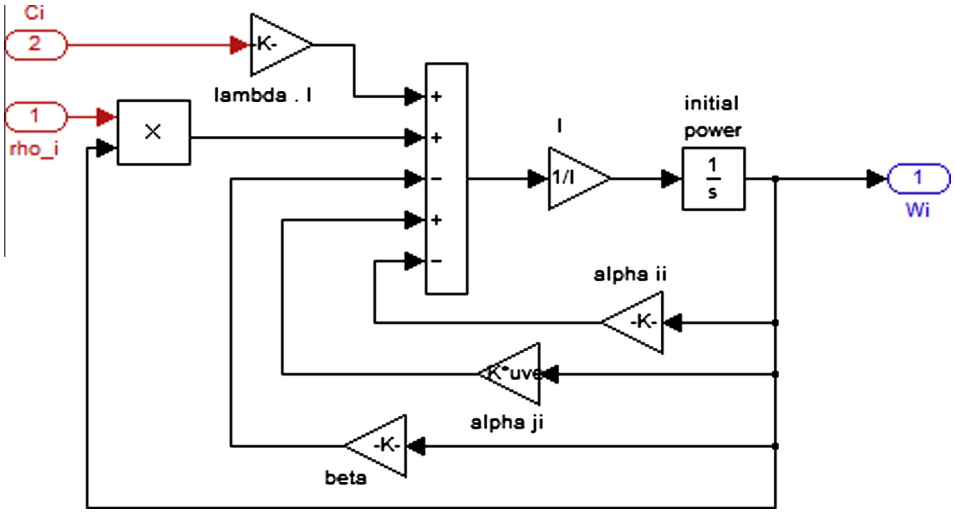

Fig. 3. Implementation of power equation.

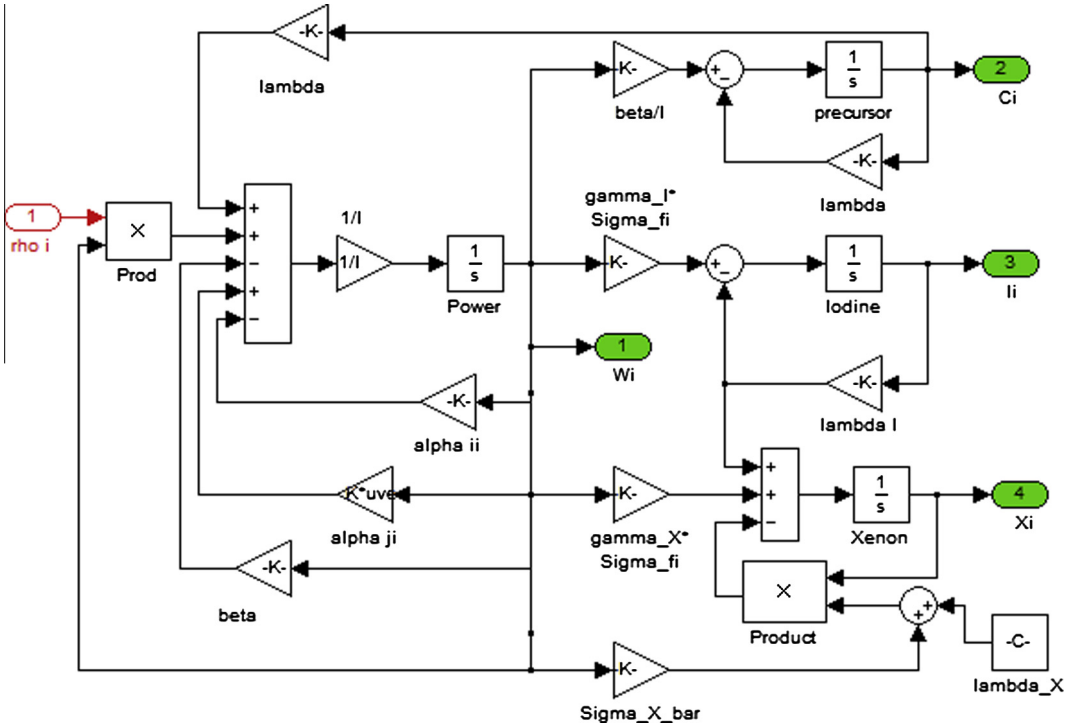

Fig. 4. Implementation of core neutronics subsystem block.

feedback for effective spatial control. Based on these considerations, let us consider the input $\mathbf{u}$ in (17) of the form

$$\mathbf{u} = -\mathbf{K}\mathbf{y} = -\mathbf{K} * \mathbf{y} \tag{27}$$

where $\mathbf{K}$ is a 4×18 matrix. With the above control, the system (17) becomes

$$\dot{\mathbf{z}} = (\mathbf{A} - \mathbf{BKM})\mathbf{z} + \mathbf{B}_f \delta q_f = \mathbf{A}\,\mathbf{z} + \mathbf{B}_f \delta q_f \tag{28}$$

where $\mathbf{A} = (\mathbf{A} - \mathbf{BKM})$. Matrices $\mathbf{A}$, $\mathbf{B}$ and $\mathbf{M}$ are given in (Shimjith et al., 2011).

5.1. Total power feedback

First consider that

$$\mathbf{K} = [\bar{\mathbf{K}}_T\ \mathbf{0}\ \cdots\ \mathbf{0}] \tag{29}$$

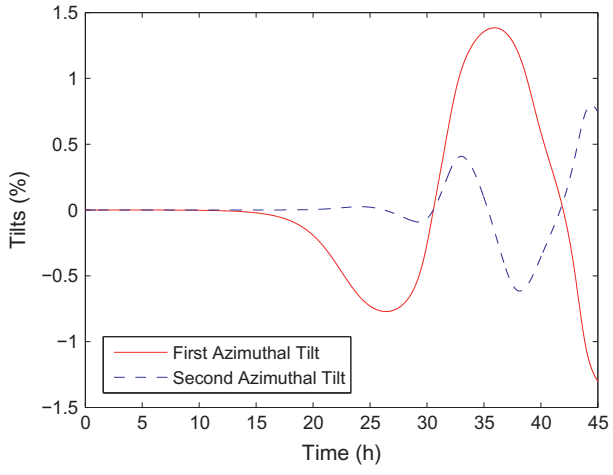

Fig. 5. Unstable modes of spatial instability.

in which $\mathbf{0}$ represents vectors of 4×1 dimension and $\bar{\mathbf{K}}_T = [K_T\ K_T\ K_T\ K_T]^T$ such that the feedback gain corresponding to total power is K_T for all RRs and is zero corresponding to nodal powers. The stability characteristic of the system (28) is investigated by varying the value of K_T and for $K_T = 12.5$, the gross behavior of the system seems stable though the system can show spatial instability. To reveal this, a transient involving a spatial power disturbance was simulated using non-linear model of the reactor given by the Eqs. (1)-(5) and (10)–(15), developed in MatLab/Simulink. It was assumed that the reactor was operating initially at full power, with control signal generated by (27). The RR2 which was initially at its equilibrium position was driven out by about 1% by giving proper control signal. Immediately after that, RR2 was driven back to its original position and thereafter left under the influence of controller. The response of the model to this disturbance was investigated in terms of variations in total reactor power and tilts in the first and second azimuthal modes defined as

$$\text{First azimuthal tilt} = \frac{W_L - W_R}{\sum_{i=1}^{17} \frac{W_i}{2}} \times 100\%$$

$$\text{where } W_L = \frac{1}{2}W_1 + \sum_{i=6}^{9} W_i + \sum_{i=14}^{17} W_i$$

$$\text{and } W_R = \frac{1}{2}W_1 + \sum_{i=2}^{5} W_i + \sum_{i=10}^{13} W_i.$$

$$\text{Second azimuthal tilt} = \frac{W_{q1} - W_{q2}}{\sum_{i=1}^{17} \frac{W_i}{2}} \times 100\%$$

$$\text{where } W_{q1} = \frac{1}{2}W_1 + W_2 + W_3 + W_6 + W_7 + W_{10} + W_{11} + W_{14} + W_{15},$$

$$\text{and } W_{q2} = \frac{1}{2}W_1 + W_4 + W_5 + W_8 + W_9 + W_{13} + W_{12} + W_{16} + W_{17}.$$

It was observed from the simulation that inspite of the global power being regulated at full power, the power distribution in the core undergoes oscillations. Within 38 h, the first and second azimuthal modes of oscillation grow to the amplitudes of the order of 1.4% and 0.75% respectively as shown in Fig. 5. Period of the

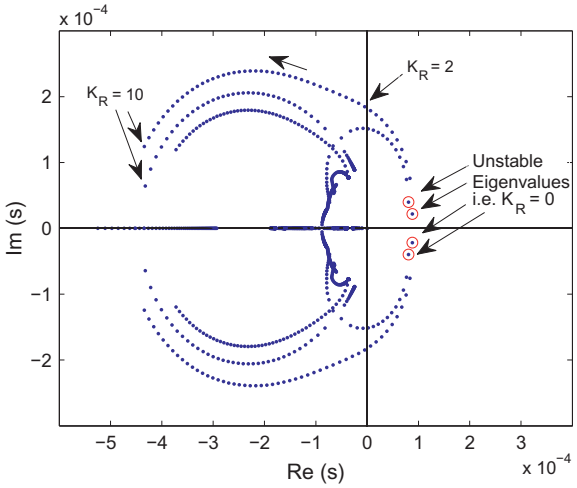

Fig. 6. Effect of feedback of nodal powers in which RRs are placed on eigenvalue locations.

oscillations are observed to be 20 h and 12 h respectively for first and second azimuthal tilts. Amplitudes of first and second azimuthal tilts are observed to be considerably higher than as given in Fig. 5, if reactivity feedback due to coolant void fraction is not considered. Moreover, if xenon reactivity feedback is removed, then no oscillations in power distribution are observed suggesting that, these are indeed xenon induced spatial oscillations. These spatial oscillations and subsequent local overpowers pose a potential threat to the fuel integrity of any nuclear reactor, and hence require control. Therefore, it is necessary to devise a suitable spatial power controller for AHWR.

5.2. Spatial power feedback

As observed in the Section 5.1, the AHWR system is showing spatial instability even with total power feedback. This is because, the system (28) has still four eigenvalues with positive real parts and three eigenvalues at origin. Hence, in addition to total power feedback, feedback of spatial power is required. A similar kind of control strategy is proposed by Shimjith et al. in (Shimjith et al., 2011), in which feedback of all the seventeen nodal powers is taken. Here, spatial stabilization of AHWR system is achieved with the feedback of nodal powers, in which RRs are placed alongwith total power feedback. Thus, in (29), **K** that was restricted to contain non-zero values only in the first column, will now be allowed to have non-zero values in other locations. This can be realized in such way that, feedback gain corresponding to total power is K_T and feedback gain to power in nodes 2, 4, 6 and 8 is K_R, that is

$$\mathbf{K}=\begin{bmatrix} K_T & 0 & K_R & 0 & 0 & 0 & 0 & 0 & 0 & 0 & 0 & 0 & 0 & 0 & 0 & 0 \\ K_T & 0 & 0 & 0 & K_R & 0 & 0 & 0 & 0 & 0 & 0 & 0 & 0 & 0 & 0 & 0 \\ K_T & 0 & 0 & 0 & 0 & 0 & K_R & 0 & 0 & 0 & 0 & 0 & 0 & 0 & 0 & 0 \\ K_T & 0 & 0 & 0 & 0 & 0 & 0 & 0 & K_R & 0 & 0 & 0 & 0 & 0 & 0 & 0 \end{bmatrix}. \tag{30}$$

Fig. 6 shows the locus of both stable and unstable eigenvalues near origin when K_R was increased progressively from zero. It is observed that, all the unstable eigenvalues are stabilized for $K_R \geqslant 2$, which proves that the feedback of nodal powers in which RRs are placed can be effectively used to stabilize the system. Most of the eigenvalues near to the origin are found to have settled at their respective new locations for $K_R \approx 10$. With this consideration value of K_R is selected as 10. Closed loop eigenvalues with $K_R = 10$ and $K_T = 12.5$ are found to be in the left half of s-plane, as listed in Table 1. This shows that, the control law (27) stabilizes the system (28) with **K** given by (30). In case of the AHWR, which is characterized by a complex high order model, spatial stabilization is thus achieved by feedback of the total reactor power and the power levels of the nodes containing regulating rods.

6. Transient simulations

Response of the controller was analyzed by simulating the nonlinear model of AHWR, given by the set of Eqs. (1)–(5) and (10)–(15)

Table 1
Closed loop eigenvalues of AHWR model.

Sr. No.	Eigenvalues	Sr. No.	Eigenvalues	Sr. No.	Eigenvalues
1	-2.8773×10^{-5}	37	-5.8834×10^{-2}	69	-1.751×10^{-1}
2	-2.8773×10^{-5}	38	-5.9364×10^{-2}	70	-1.8053×10^{-1}
3	-2.8773×10^{-5}	39	-5.966×10^{-2}	71	-1.8078×10^{-1}
4	-2.8773×10^{-5}	40	-5.9845×10^{-2}	72	-1.8221×10^{-1}
5	-4.0085×10^{-5}	41	-6.1191×10^{-2}	73	-2.6345×10^{-1}
6	-4.0237×10^{-5}	42	-6.1316×10^{-2}	74	-6.9796
7	-4.3283×10^{-5}	43–44	$(-5.9085 \pm i1.6901) \times 10^{-2}$	75	-3.2787×10^{1}
8	-4.3593×10^{-5}	45	-6.1803×10^{-2}	76	-3.3327×10^{1}
9	-6.755×10^{-5}	46	-6.1872×10^{-2}	77	-6.6584×10^{1}
10	-7.1457×10^{-5}	47	-6.235×10^{-2}	78	-6.8302×10^{1}
11–12	$(-7.6810 \pm i3.0862) \times 10^{-5}$	48	-6.2387×10^{-2}	79	-9.3652×10^{1}
13–14	$(-7.6926 \pm i3.0637) \times 10^{-5}$	49	-6.2702×10^{-2}	80	-9.4604×10^{1}
15–16	$(-2.0967 \pm i8.2771) \times 10^{-5}$	50	-6.2723×10^{-2}	81	-1.0867×10^{2}
17–18	$(-3.7556 \pm i7.6706) \times 10^{-5}$	51–52	$(-6.5120 \pm i2.2626) \times 10^{-2}$	82	-1.1704×10^{2}
19–20	$(-6.4610 \pm i5.6114) \times 10^{-5}$	53–54	$(-6.8026 \pm i2.3457) \times 10^{-2}$	83	-1.6966×10^{2}
21–22	$(-3.5386 \pm i7.7973) \times 10^{-5}$	55	-8.4982×10^{-2}	84	-1.7567×10^{2}
23–24	$(-5.6889 \pm i0.8659) \times 10^{-6}$	56	-1.1257×10^{-1}	85	-1.9496×10^{2}
25	-9.4731×10^{-5}	57	-1.3375×10^{-1}	86	-2.1109×10^{2}
26	-1.0049×10^{-4}	58	-1.4715×10^{-1}	87	-2.1903×10^{2}
27	-1.5741×10^{-4}	59	-1.4718×10^{-1}	88	-2.3590×10^{2}
28	-1.5881×10^{-4}	60	-1.4844×10^{-1}	89	-2.7162×10^{2}
29	-1.7621×10^{-4}	61	-1.5045×10^{-1}	90	-2.7625×10^{2}
30	-1.7705×10^{-4}	62	-1.5592×10^{-1}		
31	-2.3573×10^{-4}	63	-1.5602×10^{-1}		
32	-2.3586×10^{-4}	64	-1.5749×10^{-1}		
33	-2.4991×10^{-4}	65	-1.6038×10^{-1}		
34	-2.5026×10^{-4}	66	-1.6324×10^{-1}		
35	-1.5734×10^{-4}	67	-1.6339×10^{-1}		
36	-5.7761×10^{-2}	68	-1.6499×10^{-1}		

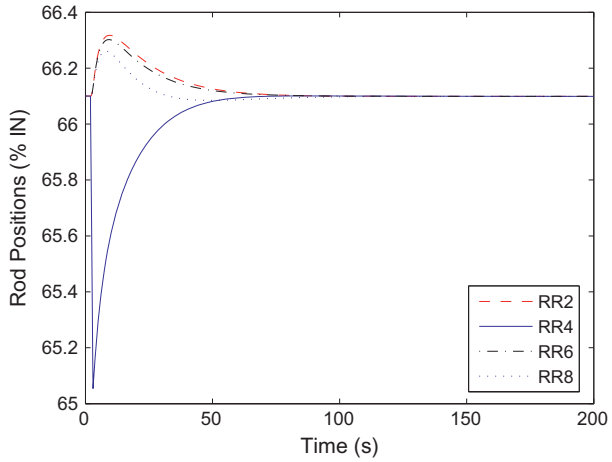

Fig. 7. RR positions during transient.

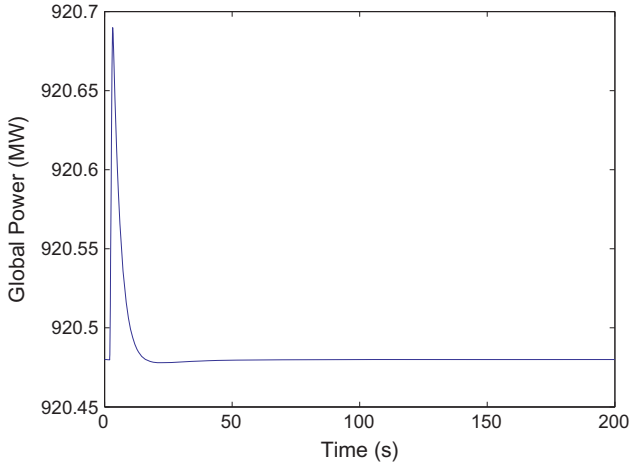

Fig. 8. Change in total reactor power subsequent to withdrawal of RR4.

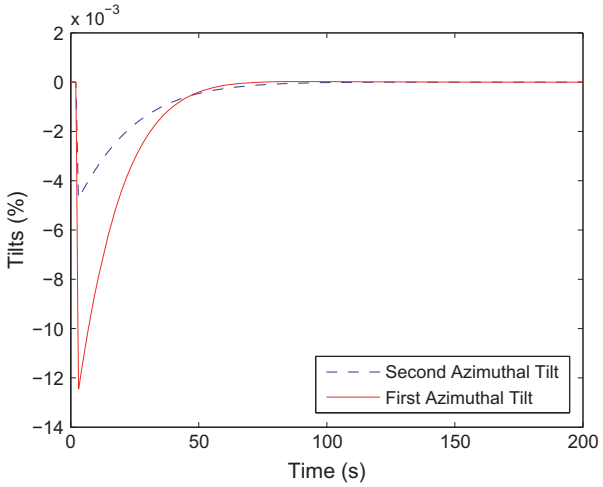

Fig. 9. Suppression of tilts.

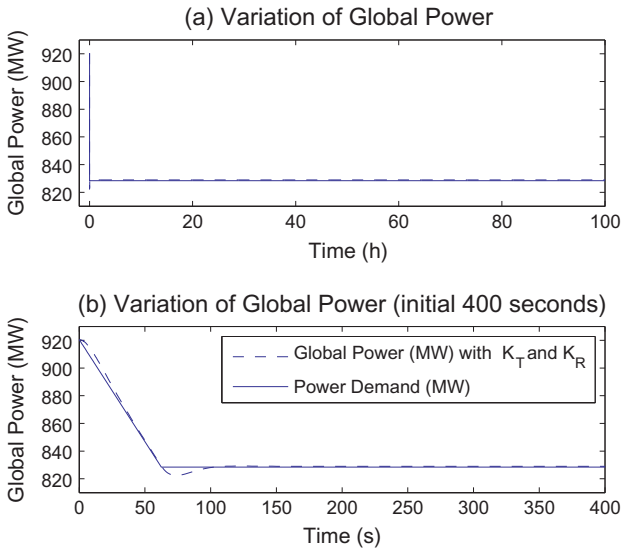

Fig. 10. Variations of global power during power maneuvering from 920.48 MW to 828.43 MW.

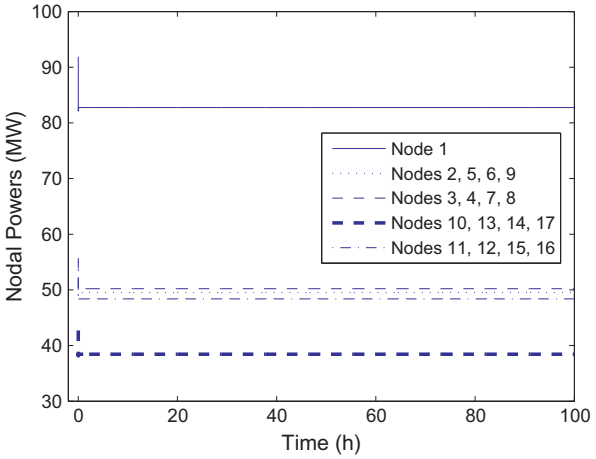

Fig. 11. Variation of nodal powers during power maneuvering from 920.48 MW to 828.43 MW.

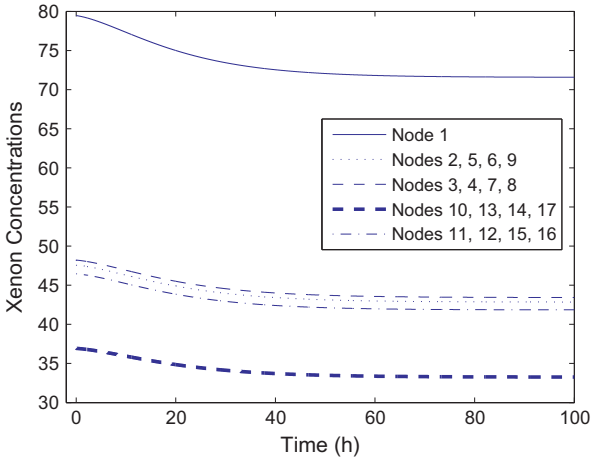

Fig. 12. Variation of xenon concentrations during power maneuvering from 920.48 MW to 828.43 MW.

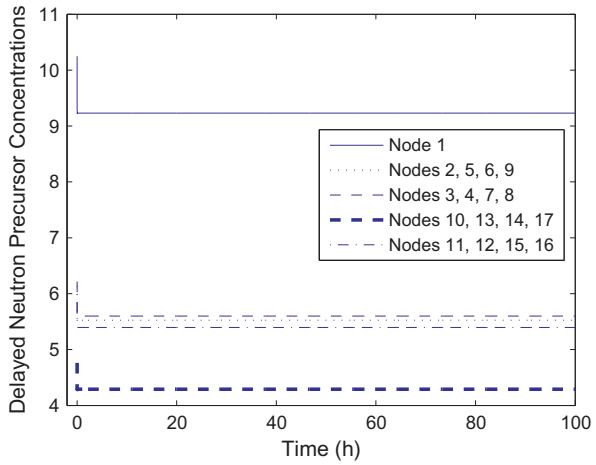

Fig. 13. Variation of delayed neutron precursor concentrations during power maneuvering from 920.48 MW to 828.43 MW.

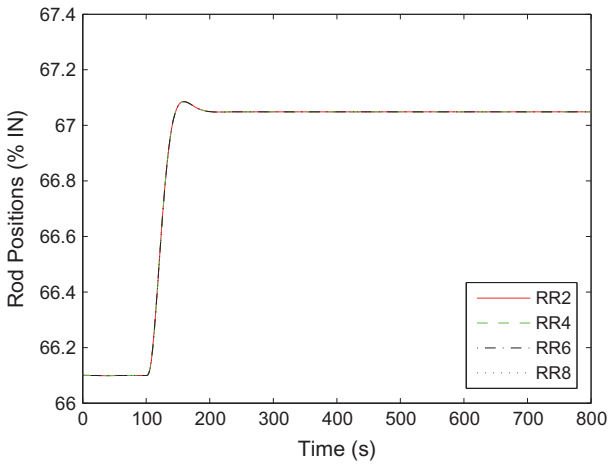

Fig. 16. Variation in RR positions due to step change in feed flow.

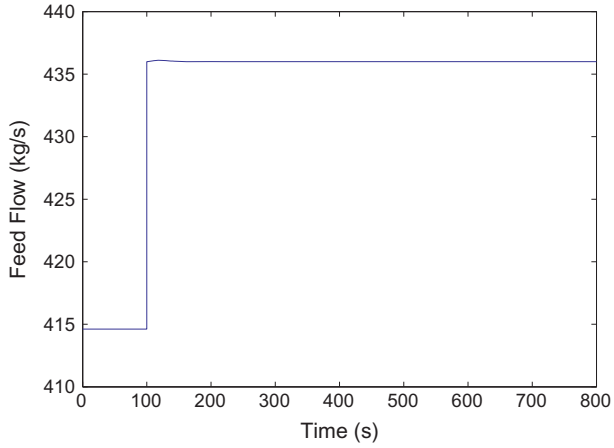

Fig. 14. Step change in the feed flow.

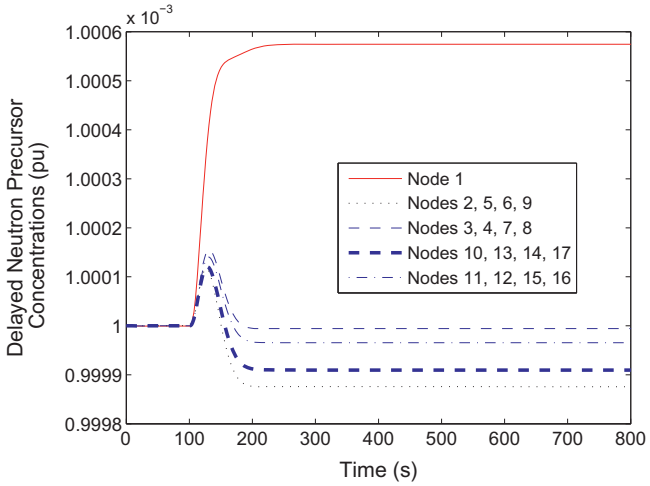

Fig. 17. Variation in delayed neutron precursor concentrations due to step change in feed flow.

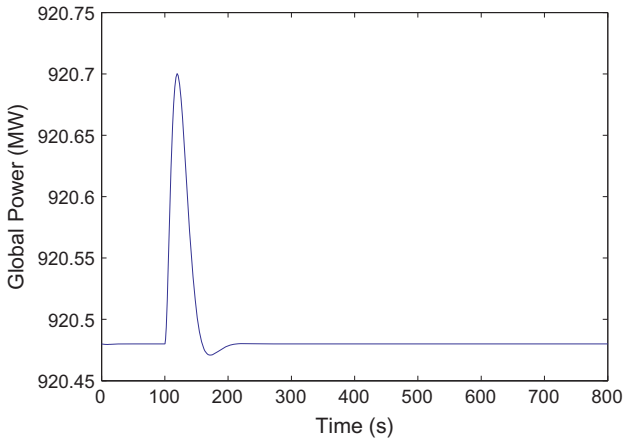

Fig. 15. Variation of total power due to step change in feed flow.

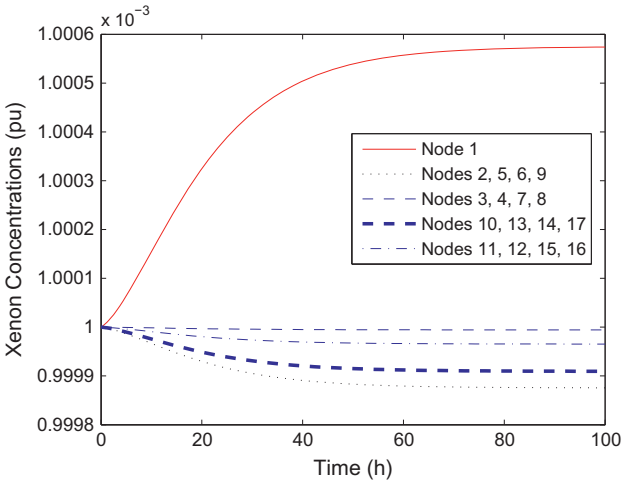

Fig. 18. Variation in xenon concentrations due to step change in feed flow.

and the control law given by (27) in MatLab/Simulink environment. Initially, it was assumed that the reactor is operating at full power equilibrium condition, with control signal generated by (30). Shortly, RR4, originally under auto control was driven out by almost 1% manually by giving proper control signal after 2 s and left under the effect of automatic control thereafter. Control signals to RR drives are generated, by computing the deviation of nodal powers in which RRs are placed, from their respective full power equivalent steady state values. From the simulation, it was observed that the RRs are driven back to their equilibrium position by the controller, as shown in Fig. 7. As a result of the controller action, disturbance in global power and spatial powers are suppressed within about 80 s. The variation in global power is depicted in Fig. 8 and variation in nodal powers, measured in terms of azimuthal tilts, are shown in Fig. 9. Since, the disturbance is of very short duration, amplitudes of first and second azimuthal tilts are respectively 0.0128% and 0.0048%.

In another transient, again the reactor is under steady state and is assumed to be operating at 920.48 MW with nodal power distributions as given in (Shimjith et al., 2011). Iodine, xenon and delayed neutron precursor concentrations are in equilibrium with the respective nodal power levels. Now, the demand is reduced uniformly at the rate of 1.5 MW/s to 828.43 MW, in approximately 61 s and held constant thereafter. During the transient, variation in global power, nodal powers, nodal xenon and delayed neutron precursor concentrations take place as shown in Fig. 10–13 respectively. From Fig. 10(a) it is observed that, during the entire course of transient the global power is maintained closed to the demand power. The global power variation during initial 400 s is depicted in Fig. 10(b). The global power is 822.42 MW approximately at 74 s and it settles within 0.12% of new demand power approximately in next 88 s. The nodal powers attain new steady state values within about 100 s as represented in Fig. 11 and do not show any variation during the remaining prolonged simulation. The xenon concentrations stabilize to their respective new steady state values in about 50 h. However, the delayed neutron precursor concentrations take just 90 s to achieve new steady state (Fig. 13). Though the difference in stabilization time for delayed neutron precursor and xenon concentrations is several hours, this does not pose any difficulty in simulation, which is accomplished in Simulink efficiently using suggested vectorization.

In order to assess the response of the system to disturbance in feed flow, non-linear model was simulated in which, reactor was operating at steady full power operation when a 5% step change was introduced in feed flow as shown in Fig. 14 after 100 s. As a result of this disturbance, global power increases from 920.48 MW to 920.70 MW and stabilizes back at its original value as shown in Fig. 15 within about next 100 s. It is evident from the Fig. 16, that in order to maintain global power at equilibrium position, all the RRs are moved inside almost by 1%. As the variation in global power is observed to be very small, only about 0.02% (Fig. 15), variations in delayed neutron precursor and xenon concentrations are also found to be very small, as indicated in Fig. 17 and 18 respectively by the per unit values. Again despite huge difference in time constants for delayed neutron precursor and xenon concentrations the simulations are carried out without any difficulty. This shows the effectiveness of the controller.

7. Conclusion

In this paper, non-linear simulation of AHWR has been carried out in MatLab/Simulink environment by vectorization of modeling equations, due to which simulation process can be simplified significantly. Steady state is achieved by the feedback of total power. From the transient simulation, it can be concluded that output feedback is able to maintain total power constant. However, total power feedback alone cannot suppress spatial oscillations/variations in the reactor core. But, this can be achieved by giving the feedback of nodal powers in which RRs are placed instead of feedback of all the nodal powers. Dynamic simulation results show the effectiveness of proposed control strategy for controlling total power alongwith xenon induced oscillations. Variations of delayed neutron precursor and xenon concentrations are also analyzed during different transient conditions. It is believed that the work carried out in this paper is very useful to control system engineers to understand the interaction between different system variables and to investigate suitable control strategy for similar other nuclear reactors.

Acknowledgements

The authors wish to express their sincere thanks to Board of Research in Nuclear Sciences (BRNS), Department of Atomic Energy, Government of India for funding the Project (Sanction No. 2009/36/102-BRNS).

References

Astrom, K.J., Bell, R.D., 2000. Drum–Boiler dynamics. Automatica 36, 363–378.
Duderstadt, J.J., Hamilton, L.J., 1975. Nuclear Reactor Analysis. John Wiley & Sons Inc., New York.
Gaikwad, A.J., Vijayan, P.K., Iyer, K., Bhartiya, S., Kumar, R., Lele, H.G., Ghosh, A.K., Kushwaha, H., Sinha, R.K., 2009. Effect of loop configuration on steam drum level control for multiple drum interconnected loops pressure tube type boiling water reactor. IEEE Trans. Nucl. Sci. 56, 3712–3725.
Javidnia, H., Jiang, J., Borairi, M., 2009. Modeling and simulation of a CANDU reactor for control system design and analysis. Nucl. Tech. 165, 174–189.
MatLab/Simulink Control Design Toolbax User Manual, 2009. Ver. 3.
Seyed, A.M.S., 2012. The simulation of a model by SIMULINK of MATLAB for determining the best ranges for velocity and delay time of control rod movement in LWR reactors. Prog. Nucl. Energy 54, 64–67.
Shimjith, S.R., Tiwari, A.P., Naskar, M., Bandyopadhyay, B., 2008. Coupled neutronics–thermal hydraulics model of advanced heavy water reactor for control system studies. Proc. IEEE INDICON, IIT Kanpur.
Shimjith, S.R., Tiwari, A.P., Bandyopadhyay, B., 2010. Space–time kinetics modeling of advanced heavy water reactor for control studies. Ann. Nucl. Energy 37, 310–324.
Shimjith, S.R., Tiwari, A.P., Bandyopadhyay, B., Patil, R.K., 2011. Spatial stabilization of advanced heavy water reactor. Ann. Nucl. Energy 38, 1545–1558.
Sinha, R.K., Kakodkar, A., 2006. Design and development of the AHWR – the Indian thorium fuelled innovative nuclear reactor. Nucl. Eng. Des 236, 683–700.
Tiwari, A.P., 1999. Modeling and Control of a Large Pressurized Heavy Water Reactor. PhD thesis, Dept. of Electrical Engg., IIT Bombay, India.